Fluid–Solid Reaction in Porous Media as a Chaotic Restart Process

Tomás Aquino, Tanguy Le Borgne, Joris Heyman

Fluid–Solid Reaction in Porous Media as a Chaotic Restart Process

Tomás Aquino,[1,2,*] Tanguy Le Borgne,[2] and Joris Heyman[2]
[1]Spanish National Research Council (IDAEA - CSIC), 08034 Barcelona, Spain
[2]Université de Rennes, CNRS, Géosciences Rennes, UMR 6118, 35000 Rennes, France

(Received 23 July 2022; revised 10 February 2023; accepted 5 June 2023; published 26 June 2023)

Chemical and biological reactions at fluid-solid interfaces are central to a broad range of porous material applications and research. Pore-scale solute transport limitations can reduce reaction rates, with marked consequences for a wide spectrum of natural and engineered processes. Recent advances show that chaotic mixing occurs spontaneously in porous media, but its impact on surface reactions is unknown. We show that pore-scale chaotic mixing significantly increases reaction efficiency compared to nonchaotic flows. We find that reaction rates are well described in terms of diffusive first-passage times of reactants to the solid interface subjected to a stochastic restart process resulting from Lagrangian chaos. Under chaotic mixing, the shear layer at no-slip interfaces sets the restart rate and leads to a characteristic scaling of reaction efficiency with Péclet number, in excellent agreement with numerical simulations. Reaction rates are insensitive to the flow topology as long as flow is chaotic, suggesting the relevance of this process to a broad range of porous materials.

DOI: 10.1103/PhysRevLett.130.264001

Chemical and biological reactions at the interface between fluid and solid phases, including adsorption, complexation, redox reactions, and precipitation or dissolution, are central to a broad range of reactive transport problems. In porous media, where the specific solid surface is high, fluid-solid reactions are at the core of a broad spectrum of processes and applications, including contaminant transport and degradation, soil remediation, mineral weathering, microbial processes, carbon dioxide sequestration, water treatment, and electrochemical processes in batteries [1–6]. Reaction kinetics are generally modeled assuming well-mixed (uniform) pore-scale reactant concentrations [7]. However, transport limitations can lead to large deviations from well-mixed estimates by reducing access of solutes to reactive surfaces [8–11]. Modeling the impact of pore-scale mixing on fluid-solid reaction kinetics remains an outstanding challenge.

Steady laminar flows through three-dimensional porous materials have been shown to spontaneously exhibit Lagrangian chaos, driving the evolution of concentration fields [12–17] and potentially impacting reaction rates. Indeed, increased surface reaction rates in unsteady chaotic flow through rotating cylinders have been observed in numerical simulations [18]. While surface reactions locally deplete reactants and limit reactivity, transport and mixing by the flow tend to reestablish reactant homogeneity within the fluid. This interplay can be modeled through delayed inter-reaction times [19] controlled by the distribution of first-passage times (FPTs) and return times of dissolved reactants to the solid interface [20–25]. Yet, the universal shape of these distributions and its link to mixing properties remain unknown.

A key property of chaotic advection is the efficient exploration of space due to the exponential divergence of nearby fluid parcels, leading to a rapid loss of dependency on initial conditions [26,27]. Thus, knowledge of reactant positions within the fluid is lost over a characteristic timescale. Here, we propose a general theory for predicting fluid-solid reactivity in chaotic flows based on a stochastic restart process [28–30]. Restart increases search efficiency [31–33], leading to enhanced reaction rates compared to purely-diffusive or nonchaotic transport. We derive new scaling laws for reaction rates as a function of Péclet number, leading to large differences compared to the predictions of current nonchaotic models. We highlight the role of viscous dissipation at solid surfaces by considering chaotic flows with slip and no-slip boundary conditions. Our results are supported by numerical simulations of reactive transport in flows through a crystalline bead pack [14] and synthetic chaotic flows [34,35].

Reactive transport system.—We consider Stokes flow through a body-centered cubic bead pack (BCC) with reactive sphere surfaces (Fig. 1). This idealized porous medium allows the intensity of chaotic mixing to be tuned by varying the mean flow orientation [14,36], permitting a systematic study of the role of chaotic mixing. To isolate the effect of chaotic mixing, we do not for the present consider more complex pore topologies such as found in rocks [37,38], where pore-scale heterogeneity induces additional transport limitations. We choose three fully-chaotic mean flow orientations, $(\theta,\phi) = (8,6)\pi/40$, $(7,5)\pi/40$, and $(5,1)\pi/40$, with increasing intensity of chaotic mixing as characterized by the infinite-time Lyapunov exponent λ_∞ [14,26]. The angle θ is defined

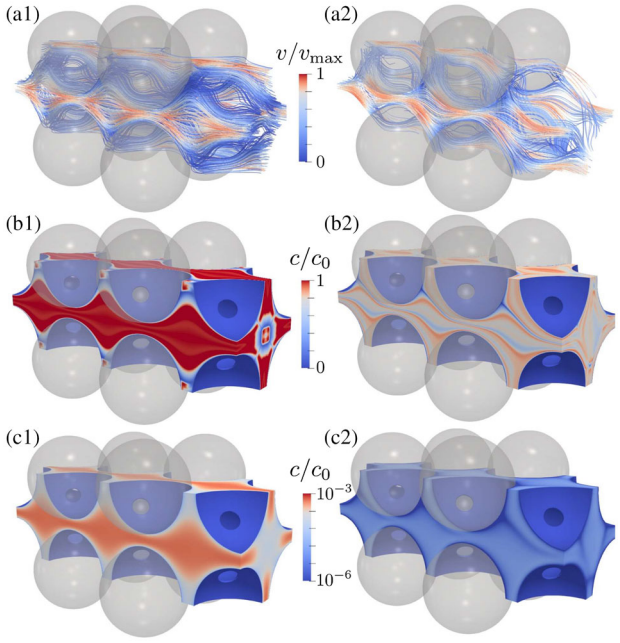

FIG. 1. Simulations of flow (line a) and fluid-solid reactive transport (lines b, c) in a BCC, for two flow orientations: $(\theta, \phi) = (0, 0)$ and $(5, 1)\pi/40$, leading to nonchaotic (column 1) and chaotic (column 2) advection. Streamlines colored with velocity magnitudes v normalized by the maximum $v_{\max}$ are shown in (a). Reactive transport of a solute instantaneously consumed at the solid surfaces (infinite Damköhler number) is shown for Péclet numbers 10^5 (b) and 10^2 (c). Initially-uniform reactant concentrations are depleted by surface reaction. Concentrations c normalized by the initial value c_0 are shown after 20 (b) and 5 (c) advection times τ_A. Chaotic flow leads to exponential fluid stretching and accelerated consumption compared to the nonchaotic case.

in the x-y plane with respect to the x direction in the primitive cell, and ϕ is the angle with the z direction. We take the cell side $\ell_c = 4r/\sqrt{3}$, where r is the sphere radius, as a reference length scale. We also consider the special case of mean flow aligned with packing symmetries, $(\theta, \phi) = (0, 0)$, which renders the flow nonchaotic.

We study transport of a single dissolved species undergoing advection–diffusion and reacting irreversibly upon contact with the fluid-solid interface according to a constant surface reaction rate k_S $[L/T]$. For a bimolecular reaction with a single solid-phase reactant at constant surface concentration c_S $[M/L^2]$, $k_S = kc_S$, with k the usual bulk reaction rate [25]. The diffusion time associated with the reference length ℓ_c is $\tau_D = \ell_c^2/(2D)$, where D is the molecular diffusion coefficient, and the reaction timescale is $\tau_R = (k_S \ell_c)^{-1}$. The Damköhler number $Da = \tau_D/\tau_R$ compares the rates of reaction and diffusion, and the Péclet number is given by $\mathrm{Pe} = \ell_c \bar{v}/D = 2\tau_D/\tau_A$, where $\bar{v}$ is the magnitude of the mean velocity and the advection time $\tau_A = \ell_c/\bar{v}$. Numerical results for reaction efficiency and FPTs use particle tracking with the approach developed in [25], based on the flow fields from [14]. Figure 1 shows Eulerian simulations of the same system for an instantaneous reaction. Computational details are given in the Supplemental Material [39].

This idealized setup allows us to isolate the impact of chaotic mixing on surface reactions. We disregard for the moment more complex effects, such as interactions between multiple reactants, reversible reactions and chemical equilibrium, and interface changes due to precipitation or dissolution. The transition to chemical equilibrium should reduce concentration gradients near the interface and therefore mitigate transport limitations. Changes in the interface are generally slow compared to transport and may be integrated in our framework through changes in the reactive surface area. The present reactive transport problem is nevertheless directly relevant to a broad range of systems, characterized by far-from-equilibrium conditions and negligible interface changes.

Enhanced reaction efficiency under chaotic mixing.—Reaction at solid surfaces locally depletes fluid reactants. Under nonchaotic flow [Figs. 1(a1)–1(c1)], transport to reactive surfaces is diffusion limited and can lead to significant reaction slowdown compared to well-mixed conditions. Under chaotic flow [Figs. 1(a2)–1(c2)], stretching and folding in the pore space redistribute the solute, increasing its probability of encounter with reactive surfaces. To quantify this effect, we define the total (or effective) reaction rate as $k_e(t) = |dM(t)/dt|/M(t)$. When the fluid reactant is well mixed, the reaction rate k_e^{wm} depends only on the diffusive flux at the interface and equals $\rho\,\mathrm{Da}/\tau_D$, where the interface-extent coefficient $\rho = \ell_c A/V$ $[-]$ encodes the interface area A per fluid volume V [25]. We define reaction efficiency as the ratio of effective to a well-mixed rate, $\varepsilon(t) = k_e(t)/k_e^{\mathrm{wm}}$ $[-]$. Under transport limitations, $\varepsilon < 1$ quantifies reaction slowdown (Fig. 2) due to reactant depletion near the interface (see Fig. 1). In the absence of chaotic mixing, efficiency is low and essentially independent of the flow rate, as diffusion is

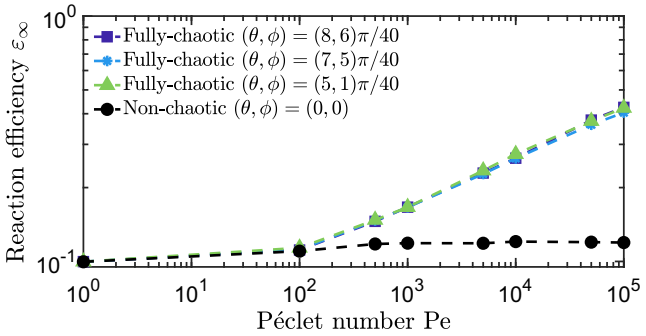

FIG. 2. Asymptotic reaction efficiency as a function of Péclet number for Stokes flow through a BCC, for Damköhler number 10^2 and four flow orientations, three yielding fully-chaotic (squares: $\lambda_\infty \approx 7.53 \times 10^{-3}$; triangles: $\approx 1.40 \times 10^{-1}$; asterisks: $\approx 2.52 \times 10^{-1}$) and one nonchaotic flow (circles).

the key mixing mechanism. Under chaotic flow, efficiency increases with flow rate and can be much larger than without chaotic mixing. Strikingly, chaotic flows with different Lyapunov exponents produce similar results. This suggests that in the presence of chaotic mixing a different process limits reaction, as discussed below.

First passage to reactive surfaces.—We first recall previous results for reaction efficiency, obtained using a chemical continuous time random walk [19] (see also Supplemental Material [39]). Within this framework, overall reaction rates are modeled in terms of interreaction times subject to stochastic delays. In order to react, the solute must first reach the reactive interface, and then return as many times as necessary for reaction to occur. Thus, reaction efficiency is dictated not only by the local surface rate k_S, but also reduced according to the statistics of FPTs and return times to the interface. In particular, the late-time efficiency depends on the mean FPT w_0 $[T]$ from the solute initial condition to the interface, on the corresponding second moment s_0^2 $[T^2]$, and on the second moment of return times [25]:

$$\varepsilon_\infty = \lim_{t\to\infty}\varepsilon(t) = \left(1 + \frac{\alpha\tau_D/w_0 + \alpha_0\rho\mathrm{Da}}{1 + \tau_D/(w_0\rho\mathrm{Da})}\right)^{-1}, \quad (1)$$

where $\alpha_0 = s_0^2/(2\tau_D w_0)$ $[-]$ and α is defined similarly for the return times. Here, we show in Supplemental Material [39] that $\alpha = w_h/\tau_D$, where w_h is the mean FPT associated with a homogeneous initial condition, removing the dependency on return times. Intuitively, w_h plays a role here because variability in return times is controlled by long trajectories, which explore the domain before returning to the interface. In the following, we quantify the impact of chaotic mixing on the FPT moments. We focus on an initial condition that is itself homogeneous ($w_0 = w_h$, $\alpha_0 = \alpha_h$). Note that solute concentrations do not remain homogeneous due to depletion around reactive surfaces (Fig. 1). Our results generalize to an arbitrary initial condition as discussed in Supplemental Material [39].

Chaotic restart.—Chaotic advection enhances mixing due to efficient Lagrangian exploration of space. We thus conceptualize chaotic mixing as a random relocation of dissolved reactants over some characteristic timescale. FPTs are modeled as diffusive FPTs subject to homogeneous spatial restart at a constant rate $k_r = \tau_r^{-1}$, where the restart time τ_r depends on flow and medium geometry. These FPTs have moments such that [33,39]

$$w_h = \frac{1-\tilde{\psi}_h^D(k_r)}{k_r\tilde{\psi}_h^D(k_r)}, \qquad \alpha_h = \frac{1 + k_r\frac{\tilde{\psi}_h^{D\prime}(k_r)}{1-\tilde{\psi}_h^D(k_r)}}{\tau_D k_r\tilde{\psi}_h^D(k_r)}, \quad (2)$$

where $\tilde{}$ denotes the Laplace transform, ψ_h is the FPT density, and ^{D} indicates pure diffusion (no flow and thus no restart). When $\tau_r \gg w_h^D$, restart is slow compared to diffusion and the latter dominates first passage: in this low-Pe regime, Taylor expansion of Eq. (2) yields $w_h \approx w_h^D$ and $\alpha_h \approx \alpha_h^D$. In the high-Pe regime, $\tau_r \ll w_h^D$, fast restart due to chaotic mixing means that only the short-time regime of diffusion is probed: only trajectories restarted close to the interface can reach it sufficiently quickly to avoid subsequent restart. Correspondingly, we show in Supplemental Material [39] that the diffusive scaling

$$\tilde{\psi}_h(\lambda) \approx \tilde{\psi}_h^D(\lambda) \approx \rho/\sqrt{2\tau_D\lambda} \quad (3)$$

holds for Laplace variable $\lambda \gg 1/w_h$ (short times $t \ll w_h$). Taylor expansion of (2) then leads to

$$w_h/\tau_D \approx \alpha_h \approx \rho^{-1}\sqrt{2\tau_r/\tau_D}. \quad (4)$$

Thus, the normalized first and second FPT moments are approximately equal under fast restart (small τ_r) and scale as $\sqrt{\tau_r}$. This holds for an arbitrary initial condition because fast restart results in a quick loss of memory. Using Eq. (1), we find a corresponding impact on reaction efficiency in the high-Péclet range:

$$\varepsilon_\infty \approx (1 + \mathrm{Da}\sqrt{2\tau_r/\tau_D})^{-1}. \quad (5)$$

In what follows, we close the model for arbitrary Pe by quantifying the dependency of τ_r on flow and geometry.

Restart time under chaotic mixing.—The restart model simplifies the mixing process by employing a constant restart rate. We find here that this leads to accurate descriptions when this rate is obtained from the slowest mechanism limiting mixing. We distinguish two scenarios for FPTs to highlight the effect of the hydrodynamics close to the interface: interfaces with (i) slip and (ii) no-slip flow conditions: (i) applies to inviscid flows and is relevant for reactions at the interface of immiscible fluids and (ii) corresponds to viscous (e.g., Stokes) flows and applies to typical flows through porous media.

When the bulk of the flow is fully chaotic, the stirring rate is proportional to the mean velocity [40]. Hence, the characteristic time scale τ_b for mixing in the bulk scales as $\tau_b/\tau_D \sim \mathrm{Pe}^{-1}$. Under slip, flow along the interface is also proportional to the mean velocity. Hence, the interface restart time $\tau_r \sim \tau_A$, so that $\tau_r/\tau_D \sim \mathrm{Pe}^{-1}$. The exact velocity profile near the interface depends on the medium and flow, but this scaling remains the same as for the bulk time τ_b. Thus, the restart theory predicts that the mean FPT scales as $w_h/w_h^D \sim \mathrm{Pe}^{-1/2}$ [Eq. (4)]. This is verified in Supplemental Material for a generalized baker's map [34,35,39].

No-slip conditions fundamentally change mixing, because low velocities near the interface become the limiting factor for advective exploration [41–43]. The corresponding timescale can be determined by examining the distance $\ell_\perp$ from the interface over which diffusive and advective

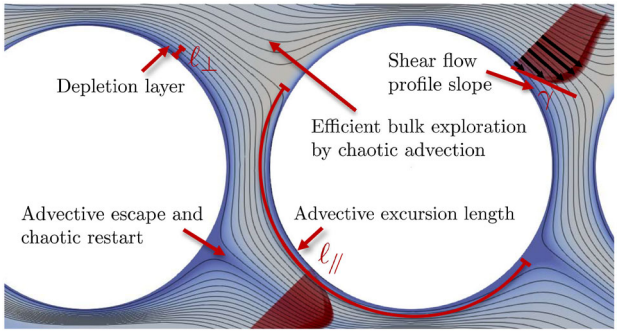

FIG. 3. Near-interface dynamics controlling the restart time in fully-chaotic, no-slip flow. Under fully-chaotic advection in the bulk, dynamics near no-slip interfaces represent the limiting factor for advection-induced exploration of the domain and set the restart time. This leads to restart times controlled by interface shear γ, which result from balancing advective and diffusive escape times near the interface.

exit rates are balanced, where reactants are likely to reach the interface before being "restarted" due to chaotic advection (Fig. 3). This distance is also the characteristic length scale of depletion for instantaneous surface reactions (see Fig. 1). Diffusive exit is controlled by diffusion perpendicular to the interface, and advective exit by flow parallel to it. Uniformly-distributed solute exits an open region of length ℓ by diffusion with an average FPT of $\ell^2/(12D)$ [20]. Diffusive exit from near the interface is one sided, so that the diffusive escape time $\tau_\perp = \ell_\perp^2/(3D)$ can be obtained by considering two-sided escape in a domain with $\ell = 2\ell_\perp$. Approaching the interface, velocity decay is characterized by an average shear rate $\gamma = \langle|\nabla v|\rangle$ $[T^{-1}]$. The average magnitude up to distance $\ell_\perp$ is $\gamma\ell_\perp/2$, and the average advective exit rate is $k_A = \gamma\ell_\perp/(2\ell_{/\!/})$, where $\ell_{/\!/}$ is the typical distance traveled in a visit. Setting $k_r = k_A = 1/\tau_\perp$,

$$\frac{\tau_r}{\tau_D} = \frac{2}{3}\left(\frac{\ell_\perp}{\ell_c}\right)^2, \qquad \frac{\ell_\perp}{\ell_c} = \left(\frac{6\ell_{/\!/}}{\ell_c\gamma_*\mathrm{Pe}}\right)^{1/3}, \tag{6}$$

where $\gamma_* = \tau_A\gamma$ $[-]$. Thus, without slip, the FPTs governing asymptotic reaction rates are controlled by interface flow shear. For large Pe, the mean FPT [Eq. (4)] scales as $w_h/w_{h,D} \sim \ell_\perp/\ell_c \sim (\gamma_*\mathrm{Pe})^{-1/3}$, a slower decay compared to inviscid flows ($\mathrm{Pe}^{-1/2}$) and to the mixing time in chaotic flows $[\ln(\lambda_\infty\mathrm{Pe})/(\lambda_\infty\mathrm{Pe})]$ [40]. The $\mathrm{Pe}^{-1/3}$ scaling is consistent with simulations as discussed below. In Supplemental Material [39], we confirm that Stokes flow past a reactive sphere forms a depletion layer whose width also follows this scaling. This is consistent with mixing under rod stirring in a beaker, where the mixing scale at which advective compression by shear and diffusive spreading are balanced follows this scaling near the interface [42].

The role of flow near the interface in setting the restart time also explains its lack of dependence on the Lyapunov exponent λ_∞. Chaotic mixing ensures efficient mixing in the bulk, but transport near the interface is limited by diffusion under shear. While reaction rates are insensitive to λ_∞, and thus to the details of the chaotic stretching and folding of material lines at the pore scale, they fundamentally differ from nonchaotic flows (Fig. 2). Under the latter, FPT moments, and therefore reaction efficiency [Eq. (1)], are diffusion limited and thus independent of Pe. In partially-chaotic flows, where chaotic regions coexist with nonchaotic islands, a transitional dependence on Péclet number following the restart prediction is observed; however, at larger Péclet, the restart model overpredicts mixing because diffusion within the islands becomes the limiting factor (see Supplemental Material [39]).

Predictions across the full Pe-Da *range.*—We estimate the restart time for the BCC and compare the resulting predictions for FPT moments and reaction efficiency to simulations. Using a typical trajectory length $\ell_{/\!/} = \pi r$ (Fig. 3), Eq. (6) yields

$$\tau_r/\tau_D = 2[\pi/(2\gamma_*\mathrm{Pe})]^{2/3}. \tag{7}$$

Figure 4(a) shows the FPT moments w_h and α_h for the three fully-chaotic orientations from Fig. 2. Predictions are obtained by inserting $k_r = \tau_r^{-1}$ according to Eq. (7) in Eq. (2). For arbitrary Péclet, the purely-diffusive FPT density ψ_h^D is computed numerically. Its mean w_h^D is the low-Pe limit of w_h, and its shape controls the intermediate-Pe regime. It does not require knowledge of flow, leading to substantial computational advantage. For high Pe, (2) simplifies to (4), which does not require ψ_h^D: predictions follow from the interface shear γ_* and interface extent ρ, without the need for transport simulations. For the BCC, $\rho \approx 14.7$ is determined analytically, and we find $\gamma_* \approx 4 \times 10^1$ numerically for all flow orientations (see Supplemental Material [39]). The predictions are in very good agreement with simulations over the full range of Péclet [Fig. 4(a)]. The moments w_h and α_h collapse at high Pe as predicted, as do all results for different flow orientations.

Figure 4(b) shows the reaction efficiency, predicted by inserting the FPT moments in Eq. (1). The chaotic restart model is in excellent agreement with simulations across the full range of Pe and Da. For low Da, $\varepsilon_\infty \approx 1$, because diffusion homogenizes reactive depletion. For low Pe and high Da, reaction is diffusion limited and $\varepsilon_\infty \sim \mathrm{Da}^{-1}$ [Eq. (1)]. Chaotic mixing counteracts this tendency by smoothing over concentrations and increasing reactant availability. This is most pronounced at high Pe and Da, for which we obtain, by inserting (7) in (5), $\varepsilon_\infty \approx \{1 + 2\mathrm{Da}[\pi/(2\gamma_*\mathrm{Pe})]^{1/3}\}^{-1}$. For $Da \geq 10$, we observe significant effects for $10^2 \leq \mathrm{Pe} \leq 10^5$, relevant for both natural porous flows and industrial applications.

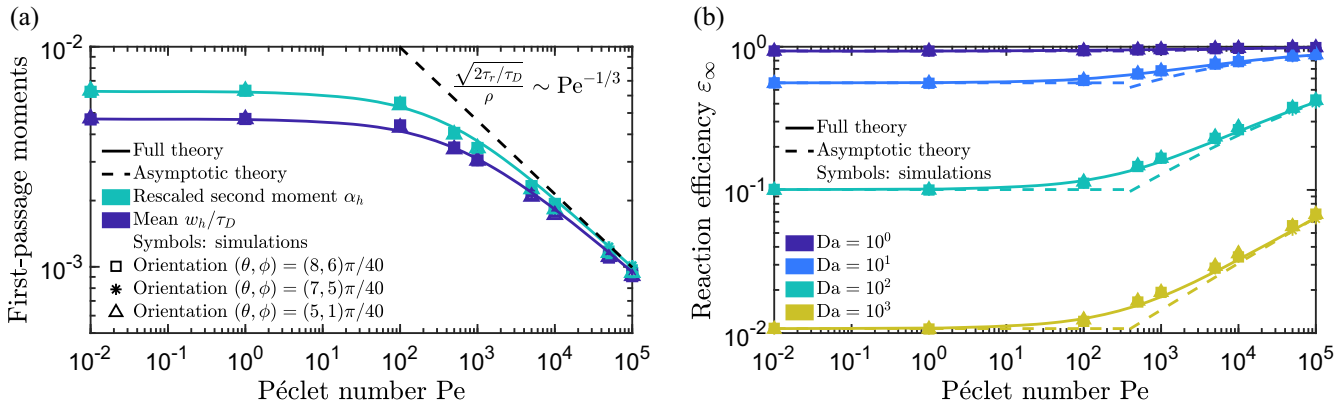

FIG. 4. Moments of first-passage times (a) and asymptotic reaction efficiency (b) as a function of Péclet number in a BCC. Symbols (superimposed) are based on numerical computation of first-passage and return times for three chaotic flow orientations. Solid lines show theoretical predictions using the restart model [Eqs. (1), (2), and (7)]. The dashed line in (a) is the large-Pe prediction using Eqs. (4) and (7). Dashed lines in (b) are small-Pe [Eq. (1) for pure diffusion] and large-Pe [Eqs. (5) and (7)] predictions, for $w_h \leqslant w_h^D$ and $\tau_r > w_h^D$, respectively.

Conclusions.—We have developed a general theory based on a stochastic restart process that quantifies the impact of chaotic flow on first-passage times to solid surfaces. The model predicts that pore-scale chaotic mixing leads to a significant enhancement of fluid-solid reaction rates compared to the nonchaotic flow paradigm, in agreement with numerical simulations. Such chaotic dynamics are increasingly observed and expected to be inherent to 3D porous media [12,15,17]. This mechanism hence likely affects reaction rates in a broad spectrum of porous materials and reactive transport applications. As long as microscale flow is fully chaotic, reaction rates are independent of the microscopic details. Hence, the predictions for effective reaction rates are expected to be general and can be linked to basic porous medium properties, such as specific surface and pore size. These findings open new avenues for understanding and modeling reactive transport dynamics in natural and engineered media, and for optimizing industrial processes involving catalysis, chromatography, and filtering.

This new theory of FPTs and their impact on reaction rates involves a stochastic restart of diffusive solute excursions to the reactive interface. By tying the restart rate to basic properties of flow and medium geometry, we predict FPT moments and reaction efficiency across Péclet and Damköhler numbers. We show that scaling exponents depend on the presence of slip or no-slip flow. This highlights the role of fluid dynamics near the interface and provides insights into the effect of chaotic flows in a broader range of reactive systems, including reactive processes at the interface of immiscible fluids. The general role of chaotic mixing is highlighted here by considering an idealized medium and a simple reaction, but the restart formulation provides a promising framework to study more complex scenarios.

This work was supported by a Marie Skłodowska Curie Individual Fellowship, funded by the European Union's Horizon 2020 research and innovation program via *ChemicalWalks* 838426 (T. A.), and by the French National Research Agency via INFLOW ANR-21-CE29-0008 (T. A. and T. L. B.) and SUCHY ANR-19-CE01-0013 (J. H.).

*tomas.aquino@idaea.csic.es

[1] C. I. Steefel, D. J. DePaolo, and P. C. Lichtner, Earth Planet. Sci. Lett. **240**, 539 (2005).
[2] K. Maher and C. Chamberlain, Science **343**, 1502 (2014).
[3] L. Li *et al.*, Earth-Sci. Rev. **165**, 280 (2017).
[4] M. Carrel, V. L. Morales, M. A. Beltran, N. Derlon, R. Kaufmann, E. Morgenroth, and M. Holzner, Water Res. **134**, 280 (2018).
[5] M. L. Szulczewski, C. W. MacMinn, H. J. Herzog, and R. Juanes, Proc. Natl. Acad. Sci. U.S.A. **109**, 5185 (2012).
[6] A. Z. Weber, M. M. Mench, J. P. Meyers, P. N. Ross, J. T. Gostick, and Q. Liu, J. Appl. Electrochem. **41**, 1137 (2011).
[7] S. L. Brantley, J. D. Kubicki, and A. F. White, *Kinetics of Water-Rock Interaction* (Springer, New York, 2008).
[8] J.-M. Vanson, A. Boutin, M. Klotz, and F.-X. Coudert, Soft Matter **13**, 875 (2017).
[9] S. Molins, D. Trebotich, L. Yang, J. B. Ajo-Franklin, T. J. Ligocki, C. Shen, and C. I. Steefel, Environ. Sci. Technol. **48**, 7453 (2014).
[10] C. Soulaine, S. Roman, A. Kovscek, and H. A. Tchelepi, J. Fluid Mech. **827**, 457 (2017).
[11] Y. Al-Khulaifi, Q. Lin, M. J. Blunt, and B. Bijeljic, Environ. Sci. Technol. **51**, 4108 (2017).
[12] D. R. Lester, G. Metcalfe, and M. G. Trefry, Phys. Rev. Lett. **111**, 174101 (2013).
[13] M. Kree and E. Villermaux, Phys. Rev. Fluids **2**, 104502 (2017).
[14] R. Turuban, D. R. Lester, J. Heyman, T. Le Borgne, and Y. Méheust, J. Fluid Mech. **871**, 562 (2019).

[15] J. Heyman, D. R. Lester, R. Turuban, Y. Méheust, and T. Le Borgne, Proc. Natl. Acad. Sci. U.S.A. **117**, 13359 (2020).
[16] M. Souzy, H. Lhuissier, Y. Méheust, T. Le Borgne, and B. Metzger, J. Fluid Mech. **891**, A16 (2020).
[17] J. Heyman, D. R. Lester, and T. Le Borgne, Phys. Rev. Lett. **126**, 034505 (2021).
[18] M. D. Bryden and H. Brenner, J. Fluid Mech. **325**, 219 (1996).
[19] T. Aquino and M. Dentz, Phys. Rev. Lett. **119**, 230601 (2017).
[20] R. Metzler, S. Redner, and G. Oshanin, *First-Passage Phenomena and their Applications* (World Scientific, Singapore, 2014).
[21] O. Bénichou, C. Chevalier, J. Klafter, B. Meyer, and R. Voituriez, Nat. Chem. **2**, 472 (2010).
[22] O. Bénichou, D. Grebenkov, P. Levitz, C. Loverdo, and R. Voituriez, Phys. Rev. Lett. **105**, 150606 (2010).
[23] A. Godec and R. Metzler, Phys. Rev. X **6**, 041037 (2016).
[24] T. Aquino and M. Dentz, Phys. Rev. E **101**, 012114 (2020).
[25] T. Aquino and T. Le Borgne, Adv. Water Resour. **154**, 103981 (2021).
[26] J.-P. Eckmann and D. Ruelle, Ergodic theory of chaos and strange attractors, in *The Theory of Chaotic Attractors*, edited by B. R. Hunt, T.-Y. Li, J. A. Kennedy, and H. E. Nusse (Springer, New York, NY, 2004), pp. 273–312.
[27] D. R. Lester, M. Dentz, and T. Le Borgne, J. Fluid Mech. **803**, 144 (2016).
[28] M. R. Evans and S. N. Majumdar, Phys. Rev. Lett. **106**, 160601 (2011).
[29] A. Chechkin and I. M. Sokolov, Phys. Rev. Lett. **121**, 050601 (2018).
[30] A. Pal and S. Reuveni, Phys. Rev. Lett. **118**, 030603 (2017).
[31] M. R. Evans and S. N. Majumdar, J. Phys. A **44**, 435001 (2011).
[32] M. R. Evans, S. N. Majumdar, and K. Mallick, J. Phys. A **46**, 185001 (2013).
[33] S. Reuveni, Phys. Rev. Lett. **116**, 170601 (2016).
[34] E. Ott and T. M. Antonsen, Jr, Phys. Rev. A **39**, 3660 (1989).
[35] A. Wonhas and J. C. Vassilicos, Phys. Rev. E **66**, 051205 (2002).
[36] R. Turuban, D. R. Lester, T. Le Borgne, and Y. Méheust, Phys. Rev. Lett. **120**, 024501 (2018).
[37] B. Bijeljic, P. Mostaghimi, and M. J. Blunt, Phys. Rev. Lett. **107**, 204502 (2011).
[38] A. Puyguiraud, P. Gouze, and M. Dentz, Water Resour. Res. **55**, 1196 (2019).
[39] See Supplemental Material at http://link.aps.org/supplemental/10.1103/PhysRevLett.130.264001 for additional details and formal derivations of key results.
[40] E. Villermaux, Annu. Rev. Fluid Mech. **51**, 245 (2019).
[41] E. Gouillart, N. Kuncio, O. Dauchot, B. Dubrulle, S. Roux, and J.-L. Thiffeault, Phys. Rev. Lett. **99**, 114501 (2007).
[42] E. Gouillart, O. Dauchot, B. Dubrulle, S. Roux, and J.-L. Thiffeault, Phys. Rev. E **78**, 026211 (2008).
[43] E. Gouillart, J.-L. Thiffeault, and O. Dauchot, Phys. Rev. Lett. **104**, 204502 (2010).